Molecular Cancer Therapeutics

Irinotecan-Induced Gastrointestinal Dysfunction and Pain Are Mediated by Common TLR4-Dependent Mechanisms

Hannah R. Wardill[1,2], Rachel J. Gibson[1,3], Ysabella Z.A. Van Sebille[2], Kate R. Secombe[2], Janet K. Coller[4], Imogen A. White[2], Jim Manavis[5], Mark R. Hutchinson[2,6], Vasiliki Staikopoulos[2], Richard M. Logan[7], and Joanne M. Bowen[2]

Abstract

Strong epidemiological data indicate that chemotherapy-induced gut toxicity and pain occur in parallel, indicating common underlying mechanisms. We have recently outlined evidence suggesting that TLR4 signaling may contribute to both side effects. We therefore aimed to determine if genetic deletion of TLR4 improves chemotherapy-induced gut toxicity and pain. Forty-two female wild-type (WT) and 42 *Tlr4* null (−/−) BALB/c mice weighing between 18 and 25 g (10–13 weeks) received a single 270 mg/kg (i.p.) dose of irinotecan hydrochloride or vehicle control and were killed at 6, 24, 48, 72, and 96 hours. Bacterial sequencing was conducted on cecal samples of control animals to determine the gut microbiome profile. Gut toxicity was assessed using validated clinical and histopathologic markers, permeability assays, and inflammatory markers. Chemotherapy-induced pain was assessed using the validated rodent facial grimace criteria, as well as immunologic markers of glial activation in the lumbar spinal cord. TLR4 deletion attenuated irinotecan-induced gut toxicity, with improvements in weight loss ($P = 0.0003$) and diarrhea ($P < 0.0001$). Crypt apoptosis was significantly decreased in BALB/c-*Tlr4*$^{-/-billy}$ mice ($P < 0.0001$), correlating with lower mucosal injury scores ($P < 0.005$). Intestinal permeability to FITC-dextran (4 kDa) and LPS translocation was greater in WT mice than in BALB/c-*Tlr4*$^{-/-billy}$ ($P = 0.01$ and $P < 0.0001$, respectively). GFAP staining in the lumbar spinal cord, indicative of astrocytic activation, was increased at 6 and 72 hours in WT mice compared with BALB/c-*Tlr4*$^{-/-billy}$ mice ($P = 0.008$, $P = 0.01$). These data indicate that TLR4 is uniquely positioned to mediate irinotecan-induced gut toxicity and pain, highlighting the possibility of a targetable gut/CNS axis for improved toxicity outcomes. *Mol Cancer Ther; 15(6); 1376–86. ©2016 AACR.*

Introduction

Irinotecan-induced gut toxicity remains a priority concern within the field of supportive care in cancer. Typically used to treat a variety of solid tumors, irinotecan can cause severe diarrhea, rectal bleeding and infection in patients, often resulting in dose reductions and treatment delays (1). Irinotecan-induced diarrhea is clinically very significant as fluid/electrolyte imbalances can lead to renal insufficiency, malnutrition, and extreme dehydration. More importantly, these side effects have severe psychological impacts for patients and significantly affect the ability to deliver optimal treatment (2). Despite both its prevalence and clinical significance, the precise mechanisms that underpin gut toxicity remain unclear and therapeutic options for patients are limited (1).

The broadly accepted pathophysiology of chemotherapy-induced gut toxicity (CIGT) comprises five continuous and overlapping phases described by Sonis (3). Although this model can be applied to most chemotherapeutic agents, each treatment modality has unique pathologic features due to differences in the metabolism and pharmacokinetics of each anticancer drug. In the case of irinotecan, its unique enterohepatic recirculation is thought to be responsible for the high levels of intestinal toxicity. Irinotecan serves as the water-soluble precursor of the lipophilic metabolite SN-38, which is formed by carboxylesterase-mediated cleavage of the carbamate bond between the camptothecin moiety and the dipiperdino side chain (4). SN-38 is glucuronidated to the non-toxic SN-38 glucuronide (SN-38G) in the liver via the uridine–diphospho–glucuronosyl transferase (UGT1A) enzyme family, which then releases SN-38G into the intestine for elimination (4). However, in the intestinal lumen, bacterial β-glucuronidases regenerate SN-38 from SN-38G (5). This unique metabolic pathway not only results in high levels of intestinal toxicity, but also highlights the key relationship between toxicity and the gut microbiome (5).

The gut microbiome has received significant attention for its role in the development of gut toxicity following chemotherapy, with documented changes in the balance of commensal and pathogenic bacteria following numerous chemotherapeutic

[1]Discipline of Anatomy and Pathology, School of Medicine, University of Adelaide, Adelaide, South Australia, Australia. [2]Discipline of Physiology, School of Medicine, University of Adelaide, Adelaide, South Australia, Australia. [3]Division of Health Sciences, University of South Australia, Australia. [4]Discipline of Pharmacology, School of Medicine, University of Adelaide, Adelaide, South Australia, Australia. [5]Adelaide Centre for Neuroscience Research and Discipline of Anatomy and Pathology, University of Adelaide, Adelaide, South Australia, Australia. [6]Australian Research Council Centre of Excellence for Nanoscale Biophotonics, Adelaide, South Australia, Australia. [7]School of Dentistry, University of Adelaide, Adelaide, South Australia, Australia.

Corresponding Author: Hannah R. Wardill, School of Medicine, University of Adelaide, s429, Medical School South, Frome Road, Adelaide 5005, South Australia, Australia. Phone: 61-8-83133787; E-mail: hannah.wardill@adelaide.edu.au

doi: 10.1158/1535-7163.MCT-15-0990

agents (5–7). In light of these findings, the interaction between the gut microbiome and innate mucosal immune system has also gained interest, with particular emphasis on the impact of Toll-like receptor (TLR) signaling (8–10). TLRs are a family of transmembrane protein receptors recognizing a diverse range of signals on exogenous and endogenous substances considered to be "dangerous," and hence warranting activation of the innate immune system for host survival (11–13). TLR4 has been most extensively characterized as it recognizes, and responds to, lipopolysaccharide (LPS) from gram-negative bacteria. We have shown that TLR4 is overexpressed in the gut during peak injury (14) and is undetectable at later time points associated with healing (15). Further, TLR4 is thought to induce an exacerbated innate immune response resulting in a heightened toxicity profile. This mechanism is particularly relevant in the setting of irinotecan-induced gut toxicity, as our preliminary *in silico* docking data indicate that SN-38 has the potential to act as a ligand for the TLR4/MD-2 complex.

TLR4 has also been hypothesized to mediate chemotherapy-induced pain through central glial activation (9), with strong clinical evidence showing that chemotherapy-induced gut toxicity is often paralleled by the symptom of pain (15, 16). This is suggestive of common underlying mechanisms. The ubiquitous involvement of the innate immune system in both chemotherapy-induced pain and gut toxicity therefore makes TLR4 a potentially overlooked candidate in the pathophysiology of these toxicities. We therefore hypothesize that TLR4-mediated signaling plays a central role in the development of irinotecan-induced gut toxicity and pain.

Materials and Methods

Animal model and ethics

The study was approved by the Animal Ethics Committee of the University of Adelaide and complied with National Health and Research Council (Australia) Code of Practice for Animal Care in Research and Training (2014). Mice were group housed in ventilated cages with three to five animals per cage. They were housed in approved conditions on a 12-hour light/dark cycle. Food and water were provided *ad libitum*.

Experimental design. All mice were on a BALB/c background. Forty-two female BALB/c-wild-type (WT) and BALB/c-*Tlr4*$^{-/-billy}$ mice ($n^{total} = 84$) weighing between 18 and 25 g (10–13 weeks) were used. WT BALB/c mice were obtained from the University of Adelaide Laboratory Animal Service (SA, Australia), and BALB/c-*Tlr4*$^{-/-billy}$ mice, back-crossed onto BALB/c for more than 10 generations, were kindly sourced from Professor Paul Foster from the University of Newcastle (NSW, Australia) and were originally sourced from Osaka, Japan (17). All BALB/c-*Tlr4*$^{-/-billy}$ mice were homozygous null mutants and hence expressed no detectable TLR4 mRNA or protein (personal communication, Mark R. Hutchinson). Mice were treated with a single 270 mg/kg intraperitoneal (i.p.) dose of irinotecan hydrochloride (kindly provided by Pharmacia/Pfizer) prepared in a sortibol/lactic acid buffer (45 mg/mL sorbitol/0.9 mg/mL lactic acid; pH 3.4; Sigma-Aldrich; D-sorbitol #S1876, lactic acid #252476), which was shown in pilot work to cause reproducible diarrhea with no mortality. Control mice received the sorbitol/lactic acid buffer only. All mice received 0.03 mg/kg of atropine subcutaneously (s.c.) immediately prior to treatment to reduce the cholinergic response to irinotecan. Mice were randomly assigned to treatment groups and killed at 6, 24, 48, 72, and 96 hours. Mice were anaesthetized using 200 mg/kg i.p. ilium sodium pentobarbital (60 mg/mL), and blood was collected from the facial vein. They were then killed via transcardial perfusion with cold, sterile 1 × PBS (pH 7.4) followed by 4% paraformaldehyde (PFA) in 0.1 mol/L PBS (pH 7.4).

Clinical assessment of gut toxicity. All mice were monitored four times daily for the presence of diarrhea and other clinical parameters. Diarrhea was quantified (by two independent assessors) using a validated grading system where 0 = no diarrhea, 1 = mild perianal staining, 2 = moderate staining covering hind legs, and 3 = severe staining covering hind legs and abdomen with continual anal leakage (18). Mice were weighed daily to track weight loss/gain. Mice were killed if they displayed $\geq$15% weight loss or significant distress and clinical deterioration, in compliance with animal ethical requirements.

Facial grimace criteria. Chemotherapy-induced pain was measured by two independent assessors, in a blinded manner, 4 times daily in all mice using the validated rodent facial grimace criteria (19), as previously published by our group (15). Briefly, the scoring method consists of five distinct criteria: orbital tightening, cheek bulge, nose bulge, ear position, and whisker position. Each criterion was scored as 0 = absent, 1 = moderate, and 2 = severe.

Tissue preparation. Gastrointestinal tract: Following anesthesia with sodium pentobarbital, mice with perfused with chilled, sterile 1 × PBS (pH 7.4). The entire gastrointestinal tract from pyloric sphincter to rectum was dissected prior to perfusion with 4% PFA and flushed with chilled 1 × PBS (pH 7.4) to remove intestinal contents. Both the small and large intestines were weighed immediately after resection. Samples (1 cm in length) of jejunum, ileum, and colon were collected and (i) drop-fixed using 10% neutral buffered saline for processing and embedding into paraffin wax, or (ii) stored in RNAlater (Sigma Aldrich; #R0901) at −20°C for molecular analyses.

Central nervous system: Mice were perfused with 4% PFA, and the vertebral column was dissected. Vertebral bodies were removed to expose the entire spinal cord. The entire spinal cord from cervical to lumbar regions was removed, and the lumbar region was prepared for further analysis (L3/L4). The mice were then decapitated and the brain was extracted. All tissue was stored in 4% PFA overnight for processing and embedding in paraffin wax.

Bacterial diversity profiling

It is well established that the gut microbiome is involved in the metabolism of irinotecan (20). To confirm both WT and BALB/c-*Tlr4*$^{-/-billy}$ contain similar bacterial profiles, the cecal contents of 12 control animals (WT $n = 6$, BALB/c-*Tlr4*$^{-/-billy}$ $n = 6$) were aseptically collected and sent for genetic sequencing at the Australian Genomics Research Facility (Brisbane, Australia).

The sequencing details are as follows: target: 341F-806R, forward primer (341F): 5′-CCTAYGGGRBGCASCAG-3′; reverse primer (806R): 5′-GGACTACNNGGGTATCTAAT-3′; read Length: 300 bp.

Bioinformatics method. Paired-end reads were assembled by aligning the forward and reverse reads using PEAR (21) (version 0.9.5).

Primers were trimmed using Seqtk (version 1.0). Trimmed sequences were processed using Quantitative Insights into Microbial Ecology (QIIME 1.8; ref. 22) USEARCH (version 8.0.1623; refs. 23, 24) and UPARSE software.

Using USEARCH tools, sequences were quality filtered, and full-length duplicate sequences were removed and sorted by abundance. Singetons or unique reads in the data were discarded. Sequences were clustered followed by chimera filtering using the "rdp_gold" database as a reference. To obtain the number of reads in each OTU, reads were mapped back to OTUs with a minimum identity of 97%. Using QUIIME, taxonomy was assigned using the Greengenes database (version 13_8, August 2013).

PEAR assembly read statistics were as follows: WT BALB/c control 59892/67175 (89.16%); BALB/c-*Tlr4*$^{-/-billy}$ control 57982/65950 (87.92%).

Histopathologic analysis

Haematoxylin and eosin (H&E) staining was performed on 5-μm sections of jejunum, ileum, and colon cut on a rotary microtome and mounted onto glass Superfrost microscope slides (Menzel-Gläser). Slides were scanned using the NanoZoomer (Hamamatsu Photonics) and assessed with NanoZoomer Digital Pathology software view.2 (Histalim). The occurrence of eight histologic criteria in the jejunum and ileum was examined to generate a total tissue injury score (25). These criteria were villous fusion, villous atrophy, disruption of brush border and surface enterocytes, crypt loss/architectural disruption, disruption of crypt cells, infiltration of polymorphonuclear cells and lymphocytes, dilation of lymphatics and capillaries, and edema. In the colon, the latter six criteria were examined. Each parameter was scored as present = 1 or absent = 0 in a blinded fashion by two independent assessors (H.R. Wardill/K.R. Secombe).

Immunohistochemistry

Immunohistochemical assessment of cellular markers of apoptosis and proliferation. Immunohistochemistry (IHC) was carried out on 5-μm sections of jejunum, ileum, and colon, cut on a rotary microtome and mounted onto FLEX IHC microscope slides (Flex Plus Detection System, Dako; #K8020). IHC analysis was performed for caspase-3 (Abcam; #ab4051), a marker of apoptosis, and Ki67 (Abcam; #ab16667), a marker of proliferation. Changes in both parameters are validated markers for altered tissue kinetics and an excellent way to assess the subclinical severity of gut toxicity (26). IHC analysis was performed using Dako reagents on an automated machine (AutostainerPlus, Dako; #AS480) following standard protocols supplied by the manufacturer. Briefly, sections were deparrafinized in histolene and rehydrated through graded ethanols before undergoing heat-mediated antigen retrieval using an EDTA/Tris buffer (0.37 g/L EDTA, 1.21 g/L Tris; pH 9.0). Retrieval buffer was preheated to 65°C using the Dako PT LINK (pretreatment module; Dako; #PT101). Slides were immersed in the buffer, and the temperature was raised to 97°C for 20 minutes. After returning to 65°C, slides were removed and placed in the Dako AutostainerPlus (Dako; #AS480) and stained following manufacturer's guidelines. Negative controls had the primary antibody omitted. Slides were scanned using the NanoZoomer (Hamamatsu Photonics) and assessed with NanoZoomer Digital Pathology software view.2 (Histalim). Apoptosis was quantified by counting the number of positively stained cells for 15 crypts. Data were presented as average positively stained cells per crypt. Ki67 data were represented as the percentage of positively staining cells relative to total cells in the intestinal crypts. Only well-oriented, non-oblique crypts were included for analysis. All staining was analyzed by two independent assessors (H.R. Wardill/K.R. Secombe).

IHC assessment of microglia and astrocyte reactivity and expression markers. Immunostaining was conducted on 5-μm sections of lumbar spinal cord (L3/4), cut on a rotary microtome, and mounted onto Superfrost microscope slides (Menzel-Gläser). IHC analysis was performed for astrocytic Glial Fibrillary Acidic Protein (GFAP), Clone 6F2 (DakoCytomation, Dako; #M0761) and microglial Iba-1 (Wako; #019-19741). Briefly, sections were dewaxed on a hot-air blower and in xylene, then dehydrated in 100% ethanol before being quenched for endogenous peroxidase activity with 0.5% hydrogen peroxide in methanol for 30 minutes. Slides were then washed in 0.1 mol/L PBS (pH 7.4, 2 × 3 minutes) before being subjected to heat-mediated antigen retrieval using 0.1 mol/L citrate buffer (pH 6.0). Non-specific binding was blocked by 3% normal horse serum (NHS; Sigma-Aldrich) for 30 minutes at room temperature. Primary antibodies were applied, using 3% NHS as the diluent, overnight at room temperature in a humid chamber (GFAP 2 μg/mL; Iba-1 0.1 μg/mL). Following incubation with the primary antibody, a secondary goat biotinylated anti-mouse/rabbit IgG (6 μg/mL) was applied to sections for 30 minutes at room temperature (Vector Laboratories; anti-mouse #BA-9200; anti-rabbit #BA-1000). After a further PBS wash (2 × 3 minutes), slides were incubated with Pierce streptavidin peroxidase conjugate at 2 μg/mL (ThermoFisher Scientific; #21130) for 30 minutes at room temperature followed by another rinse with 0.1 mol/L PBS. The immunocomplex was then visualized with precipitation of DAB (Sigma-Aldrich; #D-5637) in the presence of hydrogen peroxide (3%). Slides were washed to remove excess DAB and lightly counterstained with haematoxylin, dehydrated, and mounted with DePeX from histolene. Slides were scanned using the NanoZoomer (Hamamatsu Photonics) and assessed with NanoZoomer Digital Pathology software (Histalim). Staining was assessed in the dorsal column of the lumbar spinal cord using ImageJ 1.49 software and the validated color deconvolution method (27).

IHC assessment of blood–brain barrier permeability. IHC analysis was also performed on 5-μm sections of brain, cut (midsagitally) on a rotary microtome, and mounted onto Superfrost microscope slides (Menzel-Gläser). Immunostaining was performed using a rabbit polyclonal anti-human albumin antibody (Dako; #A0001) as per the method described in. No antigen retrieval was required. Staining was assessed using a semiquantitative grading system, where 0 = no staining, 1 = mild staining with leakage localized to one region, 2 = moderate staining with two unrelated sites of leakage, and 3 = intestine staining with ≥3 unrelated sites or global leakage. Staining was assessed in a blinded fashion by two independent assessors (H.R. Wardill and J. Manavis).

Assessment of *in vivo* intestinal permeability

FITC-dextran assay. Three hours prior to kill time points, mice received a 500 mg/kg dose (75 mg/mL) of 4-kDa fluorescein isothiocyanate (FITC)-dextran (Sigma-Aldrich; #46944) via oral gavage. Blood was collected from the facial vein into Multivette 600 Serum-Gel with Clotting Activator capillary tubes (Sarstedt; #15.1670.100) and stored on ice for 30 minutes. Samples were

Table 1. Mean percentage of each cecal bacterial phyla in vehicle-treated WT and *Tlr4*$^{-/-}$ null mice

Phylum	WT	*Tlr4*$^{-/-}$	*P*
Bacteroidetes	22.45 ± 6.00	24.34 ± 3.01	0.79
Firmicutes	76.65 ± 5.98	71.33 ± 2.66	0.46
Proteobacteria	0.43 ± 0.12	1.93 ± 0.61	**0.05**
TM7	0.10 ± 0.06	0.56 ± 0.16	**0.03**
Actinobacteria	0.25 ± 0.09	0.65 ± 0.19	0.09
Cyanobacteria	0.02 ± 0.01	0.10 ± 0.04	0.08
Acidobacteria	0.002 ± 0.001	0.0004 ± 0.0003	0.26
Verrucomicrobia	0.0005 ± 0.0005	0.13 ± 0.11	0.27
Deferribacteres	0.005 ± 0.003	0.0006 ± 0.0003	0.23
Tenericutes	0.02 ± 0.02	0.92 ± 0.53	0.13
Chloroflexi	0.02 ± 0.005	0.01 ± 0.01	0.58
Nitrospirae	0.003 ± 0.001	0.003 ± 0.002	0.70

NOTE: Bold type indicates statistical signficance.

centrifuged at 11,000 × *g* for 5 minutes at room temperature, and the serum was isolated. Serum samples were diluted 1:3 with 1 × PBS and quantified using the BioTek Synergy Mx Microplate Reader (BioTek) and Gen5 version 2.00.18 software relative to a standard curve (range, 0.0001–10 μg/mL).

Serum Limulus Amebocyte Lysate (LAL) endotoxin assay. The LAL endotoxin assay was run on serum samples isolated from blood collected from the facial vein into Multivette 600 Serum-Gel with Clotting Activator capillary tubes (Sarstedt; #15.1670.100). The LAL QCL-1000 endotoxin detection kit (Lonza; #50-647U, 50-648U) was then used to quantify serum endotoxin, as per manufacturer's guidelines. Endotoxin concentration was determined relative to a linear standard curve (range, 0.1–1 EU/mL).

Tissue cytokine protein quantification

Protein extraction. Irinotecan causes global gastrointestinal damage; however, damage is typically most severe in the ileum and colon. Proinflammatory cytokine expression was therefore assessed using 30 mg of ileal and colonic tissue samples. Intestinal tissue samples were homogenized at room temperature using the QIAGEN TissueLyser LT (Qiagen) for 5 minutes at 50 Hz in 500 μL of the Radio-Immunoprecipitation Assay (RIPA) buffer (150 mmol/L NaCl, 1.0% IGEPAL CA-630, 0.5% sodium deoxycholate, 0.1% SDS, and 50 mmol/L Tris, pH 8.0; Sigma Aldrich; #R0278) supplemented with Roche protease inhibitor cocktail (Sigma Aldrich; #04693116001). Homogenates were centrifuged at 11,000 × *g* for 15 minutes at 4°C and the supernatant isolated, aliquoted, and stored at −80°C. Total protein concentration was quantified using the Pierce BCA Protein Assay Kit (ThermoFisher Scientific; #23225). A working concentration of 1 mg/mL was used for cytokine analysis.

Luminex multiplex cytokine assay. Cytokine concentration was measured in individual ileal and colonic homogenates using Luminex xMAP technology (Milliplex Mouse Cytokine Kit, Merck Millipore; #MPMCYTOMAG70K08) as per the manufacturer's instructions. The cytokines analyzed were: IL1β, IL6, TNFα, IL10, IFNγ, IL2, IL17α, and MCP-1. Each 96-well plate included a 6-point standard curve and two quality controls provided by Merck Millipore.

Statistical analysis

Data were compared using Prism version 7.0 (GraphPad Software). A D'Agostino–Pearson omnibus test was used to assess

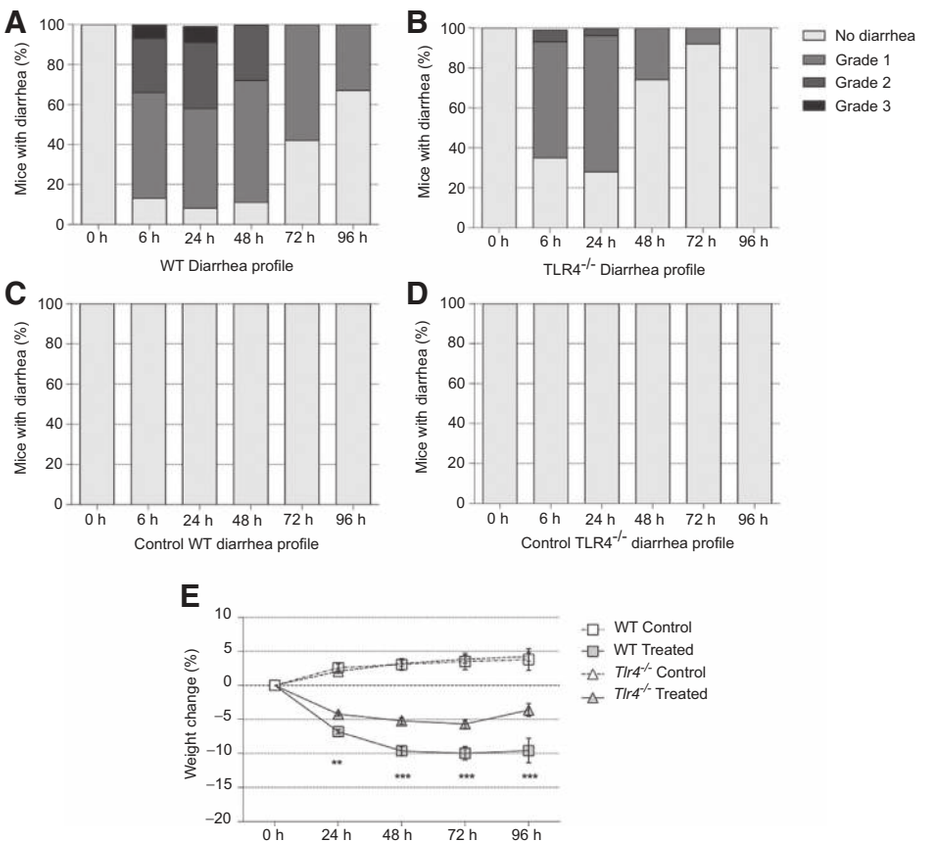

Figure 1.
Tlr4$^{-/-}$ attenuates symptomatic parameters of gut toxicity: diarrhea and weight loss. Diarrhea profiles shown for WT BALB/c mice (A) and BALB/c-*Tlr4*$^{-/-billy}$ mice (B) treated with 270 mg/kg of irinotecan, as well as vehicle-treated controls (C and D). Diarrhea data are expressed as a percentage of total animals (per time point) with a particular grade of diarrhea. Data were analyzed using a χ^2 test. Diarrhea was most significant at 24 hours after treatment in both treatment groups. Diarrhea was significantly improved in BALB/c-*Tlr4*$^{-/-billy}$ mice compared with WT (***, $P < 0.0001$). E, weight loss over the 96-hour time course. Data displayed as a percentage of weight change from baseline (0 hours). A Kruskal–Wallis with *post hoc* testing was performed to identify statistical significance. BALB/c-*Tlr4*$^{-/-billy}$ mice had significantly less body weight loss at 24 hours (**, $P = 0.003$), 48, 72, and 96 hours (***, $P < 0.0001$).

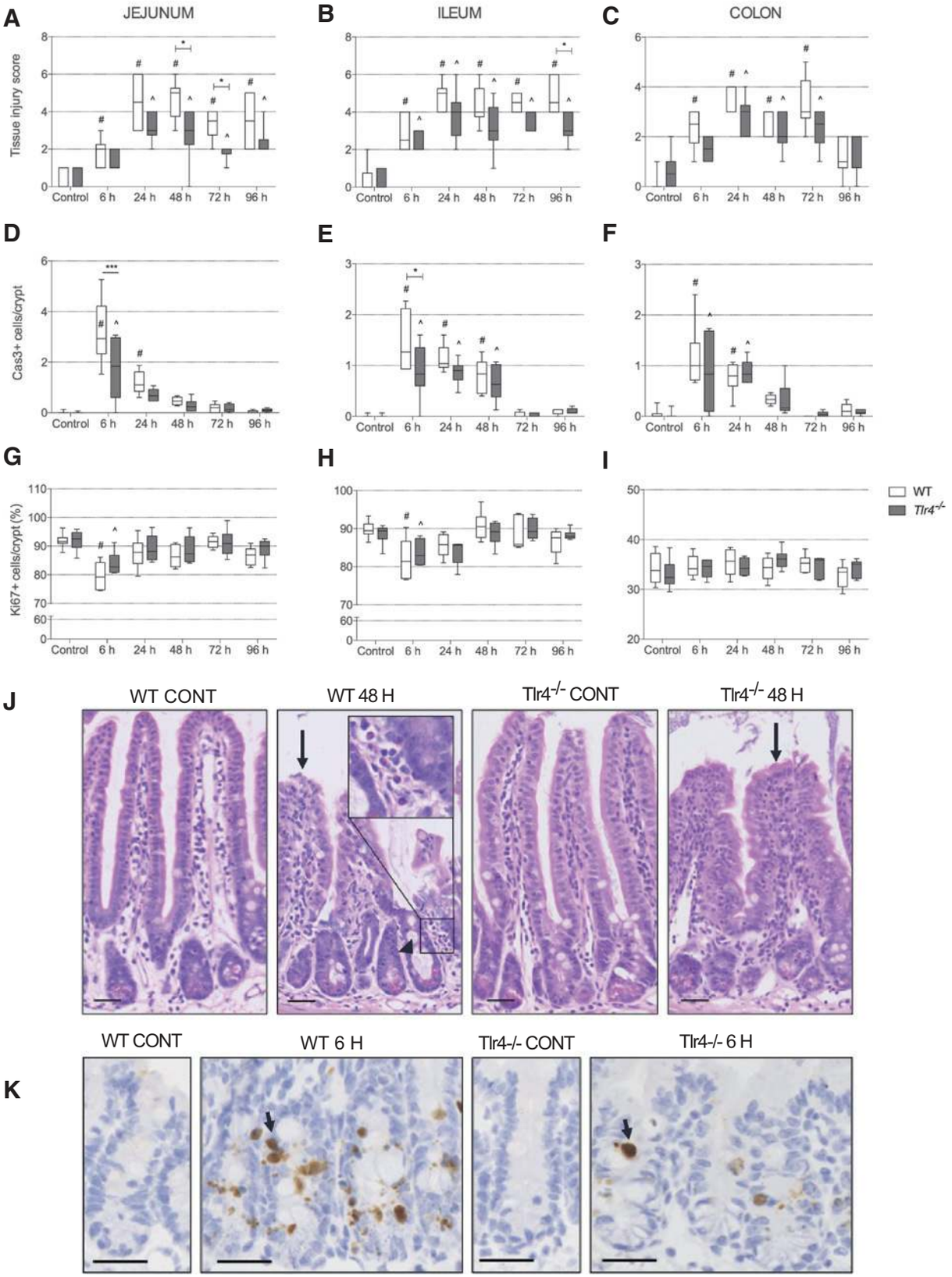

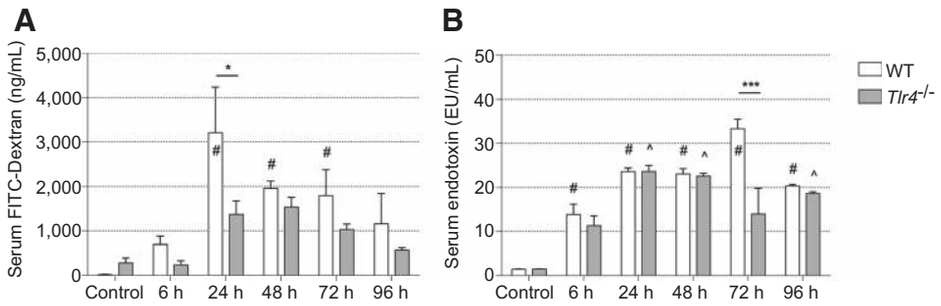

Figure 3.

Ex vivo markers of barrier permeability, serum 4 kDa FITC-dextran (A) and serum endotoxin (B). FITC-dextran was administered as a 500 mg/kg dose, via oral gavage, 3 hours prior to kill time point. Serum endotoxin was assessed using the Serum Limulus Amebocyte Lysate (LAL) endotoxin assay. Data are expressed as mean ± SEM and were analyzed using a two-way ANOVA with Tukey *post hoc*. Both markers of barrier disruption show elevations following treatment with irinotecan (#, a change from baseline in WT mice; ^, a change from baseline in BALB/c-*Tlr4*$^{-/-billy}$ mice, where $P < 0.05$). Maximum FITC-dextran permeability coincides with peak diarrhea in WT animals (24 hours). At this time point, TLR4 deletion decreased serum FITC-dextran levels (*, $P = 0.0104$) compared with WT. Serum endotoxin, indicative of LPS translocation, was reduced in BALB/c-*Tlr4*$^{-/-billy}$ mice at 72 hours compared with WT mice treated with irinotecan (***, $P = 0.0001$).

normality. When normality was confirmed, a two-way analysis of variance (ANOVA) with appropriate *post hoc* testing was performed to identify statistical significance between groups. In other cases, a Kruskal–Wallis test with the Dunn multiple comparisons test and Bonferroni correction was performed. Diarrhea data were assessed using a χ^2 test (28). A P value of <0.05 was considered statistically significant.

Results

Bacterial diversity profiling

Bacterial profiling showed comparable microbiome composition in both WT and BALB/c-*Tlr4*$^{-/-billy}$ mice (Table 1). The majority of the microbiome comprised Fermicutes (WT 76.66% ± 5.98%; BALB/c-*Tlr4*$^{-/-billy}$ 71.33% ± 2.66%) and Bacteroidetes (WT 22.46% ± 6.01%; BALB/c-*Tlr4*$^{-/-billy}$ 24.34% ± 3.00%) phyla. A two-tailed *t* test with Welch correction showed increased expression of the Proteobacteria and TM7 phyla in BALB/c-*Tlr4*$^{-/-billy}$ mice (Proteobacteria: WT 0.44% ± 0.12%; BALB/c-*Tlr4*$^{-/-billy}$ 1.93% ± 0.61%, $P = 0.046$; TM7: WT 0.10% ± 0.06%; BALB/c-*Tlr4*$^{-/-billy}$ 0.55% ± 0.16%, $P = 0.028$).

BALB/c-*Tlr4*$^{-/-billy}$ mice have attenuated clinical manifestations of irinotecan-induced gut toxicity

Irinotecan caused diarrhea in all mice from as early as 6 hours (Fig. 1A and B). Diarrhea severity was significantly improved in BALB/c-*Tlr4*$^{-/-billy}$ mice compared with WT (*, $P < 0.0001$). No diarrhea was seen in any vehicle control animals (Fig. 1C and D). Weight loss following irinotecan treatment was most severe at 72 hours in WT (−9.96% ± 0.98% from baseline) and *Tlr4*$^{-/-}$ mice (−5.68% ± 0.64% from baseline), the weight loss in BALB/c-*Tlr4*$^{-/-billy}$ mice was significantly less than that seen in WT (*, $P < 0.0001$; Fig. 1E).

BALB/c-*Tlr4*$^{-/-billy}$ mice have improved histologic architecture in the small intestine

BALB/c-*Tlr4*$^{-/-billy}$ mice treated were protected against irinotecan-induced mucosal tissue injury most effectively in the jejunum (Fig. 2A), with improvements seen in BALB/c-*Tlr4*$^{-/-billy}$ mice compared with WT at 48 (*, $P = 0.003$) and 72 hours (*, $P = 0.023$). Despite improvements in diarrhea, architectural tissue injury remained evident at 96 hours in the jejunum (Fig. 2A; WT, #, $P < 0.0001$; BALB/c-*Tlr4*$^{-/-billy}$, ^, $P = 0.003$) and ileum (Fig. 2B, WT, #, $P < 0.0001$; BALB/c-*Tlr4*$^{-/-billy}$, ^, $P < 0.0001$). This late histopathology was not evident in the colon (Fig. 2C$P > 0.05$), suggesting that colonic histopathology may be more indicative of diarrhea severity. Representative images (Fig. 2J) show villus blunting/fusion (arrow), crypt disruption (arrowhead), and inflammatory infiltrate (subset panel).

Peak apoptosis was seen at 6 hours in both WT and BALB/c-*Tlr4*$^{-/-billy}$ mice (Fig. 2D–F) with a parallel decrease in proliferation seen in the jejunum and ileum (Fig. 2G and H). BALB/c-*Tlr4*$^{-/-billy}$ mice had reduced apoptotic counts at 6 hours in the jejunum (Fig. 2D; ***, $P < 0.0001$) and ileum (Fig. 2E; *, $P = 0.002$). Representative immunostaining (Fig. 2K) shows crypt caspase-3–positive cells in the jejunal crypts. No change was seen in proliferation between WT and BALB/c-*Tlr4*$^{-/-billy}$ mice in any region at any time point ($P > 0.05$; Fig. 2G–I).

TLR4-dependent signaling contributes to intestinal barrier disruption

Serum FITC-dextran was elevated in WT mice at 24 (#, $P < 0.0001$), 48 (#, $P = 0.0043$), and 72 hours (#, $P = 0.01$) compared with vehicle controls (Fig. 3A), indicating compromised intestinal barrier function. No statistically significant change was seen in BALB/c-*Tlr4*$^{-/-billy}$ mice at any time point ($P > 0.05$). At 24 hours

Figure 2.

Histopathologic parameters in jejunum, ileum, and colon of WT and BALB/c-*Tlr4*$^{-/-billy}$ mice. There were significant increases in tissue injury scores in WT and BALB/c-*Tlr4*$^{-/-billy}$ mice in the jejunum (A), ileum (B), and colon (C); #, a change from baseline in WT mice, where $P < 0.05$; ^, a change from baseline in BALB/c-*Tlr4*$^{-/-billy}$ mice, where $P < 0.05$. Data presented as interquartile range ± mix/max. TLR4 deletion reduced the severity of jejunal and ileal tissue damage (A; *, $P = 0.003$ 48 hours, *, $P = 0.023$ 72 hours); B *, $P = 0.005$ 96 hours). Apoptosis was increased in the jejunum (D), ileum (E), and colon (F) in all treated animals ($P < 0.05$). TLR4 deletion attenuated apoptosis in the jejunum and ileum (D: ***, $P < 0.0001$, 6 hours; E: *, $P = 0.0023$ 6 hours). Decreased small intestinal proliferation was noted at 6 hours in all animals treated with irinotecan (G and H); however, no differences were seen between WT and BALB/c-*Tlr4*$^{-/-billy}$ mice. No change was seen in the colon (I). Representative histological (J) and caspases-3 immunostaining (K) show clear jejunal tissue injury at 48 hours characterized by crypt ablation (arrowhead), villous blunting/fusion (arrow), inflammatory infiltrate (subset panel), and crypt apoptosis at 6 hours [brown staining (arrow); K]. Scale bars, 30 μm. Original magnification, ×40.

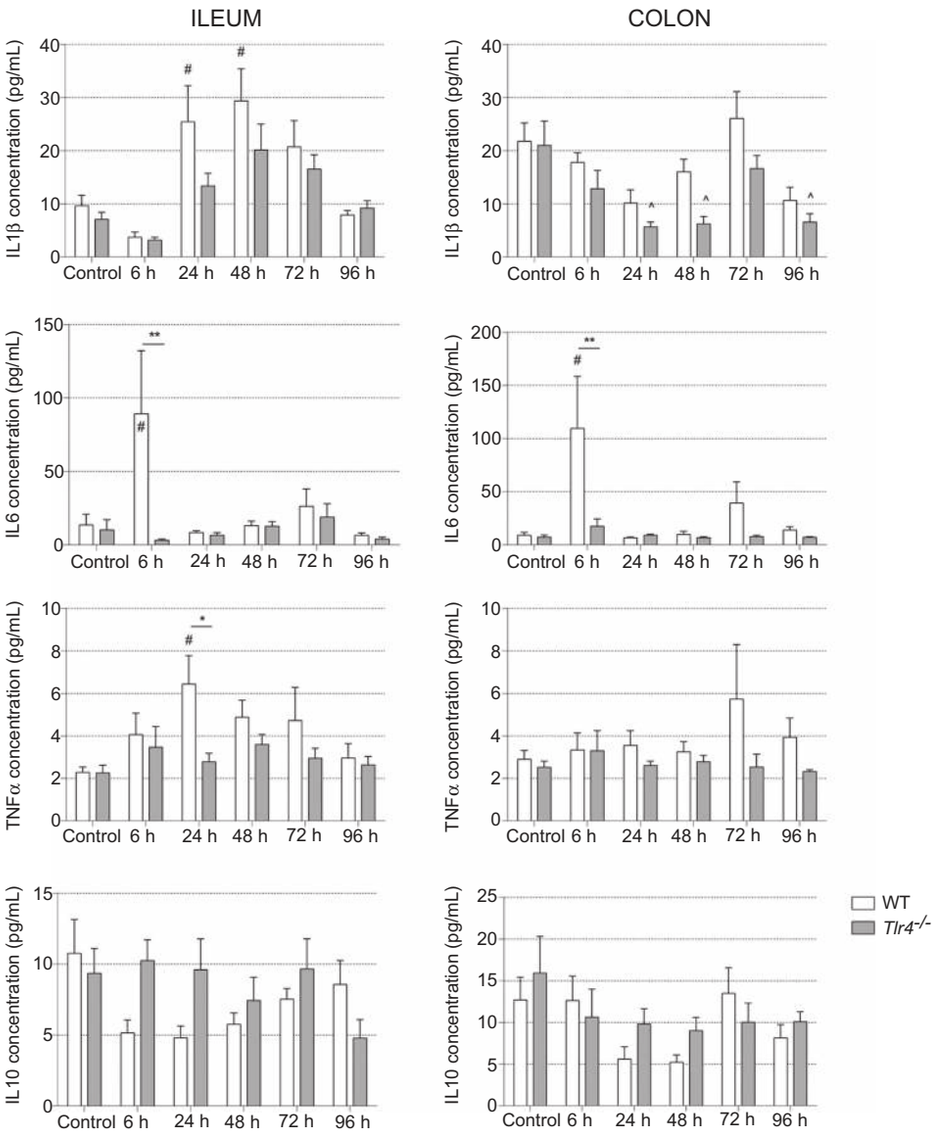

Figure 4.
Cytokine expression in the ileum and colon. Cytokine expression was assessed using Luminex xMAP technology. Data, mean ± SEM (pg/mL). A two-way ANOVA with Tukey *post hoc* was performed to identify statistical significance. IL1β expression increased in the ileum of WT animals treated with irinotecan compared with control (#, $P = 0.0394$, 24 hours; #, $P = 0.0036$, 48 hours). Only a significant decrease was seen in BALB/c-*Tlr4*$^{-/-billy}$ mice (#, a change from baseline in WT mice; ^, a change from baseline in BALB/c-*Tlr4*$^{-/-billy}$ mice, where $P < 0.05$). BALB/c-*Tlr4*$^{-/-billy}$ mice lacked an IL6 response at 6 hours, with significantly lower expression compared with WT mice (**, $P = 0.0002$ ileum; **, $P = 0.0005$ colon). TNFα expression peaked at 24 hours in the ileum of WT mice treated with irinotecan (#, $P = 0.0113$). This was significantly elevated relative to BALB/c-*Tlr4*$^{-/-billy}$ mice (*, $P = 0.0166$), which showed no elevation in TNFα ($P > 0.05$). No change was seen in the anti-inflammatory cytokine IL10.

after irinotecan, WT mice had significantly greater serum FITC-dextran concentrations compared with BALB/c-*Tlr4*$^{-/-billy}$ mice (3209.59 ± 1020.88 ng/mL vs. 1373.97 ± 303.56 ng/mL; *, $P = 0.01$).

Serum endotoxin (LAL), a measure of LPS translocation, was elevated at all time points in WT mice treated with irinotecan (#, $P < 0.005$), with most significant peaks at 24 and 72 hours (both #, $P < 0.0001$; Fig. 3B). Serum endotoxin was highest at 24 (^, $P = 0.001$), 48 (^, $P = 0.003$), and 96 hours (^, $P = 0.02$) in BALB/c-*Tlr4*$^{-/-billy}$ mice treated with irinotecan compared with control. There was a significant difference in serum endotoxin between WT and BALB/c-*Tlr4*$^{-/-billy}$ mice at 72 hours after irinotecan treatment (33.35 ± 2.19 EU/mL vs. 13.96 ± 5.87 EU/mL; ***, $P < 0.0001$).

BALB/c-*Tlr4*$^{-/-billy}$ mice exhibit a muted inflammatory response

BALB/c-*Tlr4*$^{-/-billy}$ mice treated with irinotecan showed no statistically significant increase in IL1β, IL6, or TNFα expression in the ileum or colon when compared with vehicle controls (Fig. 4). There were significant increases in the expression of IL1β in the ileum of WT mice treated with irinotecan (#, $P = 0.04$, 24 hours; #, $P = 0.004$, 48 hours). No statistically significant increase was seen in TLR4-deficient mice (Fig. 4; $P > 0.05$). BALB/c-*Tlr4*$^{-/-billy}$ mice lacked the IL6 response seen in WT animals at 6 hours (#, $P = 0.003$, *, $P = 00002$ ileum; #, $P = 0.0004$, *, $P = 0.0005$ colon; Fig. 4). WT mice also showed increased ileal expression of TNFα (#, $P = 0.01$) 24 hours after treatment with irinotecan, and this was significantly elevated relative to treated BALB/c-*Tlr4*$^{-/-billy}$ mice (*, $P = 0.02$). No change was seen in IL10.

Irinotecan-induced pain is associated with TLR4-dependent astrocytic GFAP expression

Facial grimace criteria peaked at 6 hours in both treated animal groups, reducing steadily for the remainder of the experimental time course (Fig. 5A). From 6 to 72 hours, BALB/c-*Tlr4*$^{-/-billy}$ mice had reduced facial grimace criteria compared with WT mice (***, $P < 0.0001$). Elevated GFAP staining, indicative of astrocyte

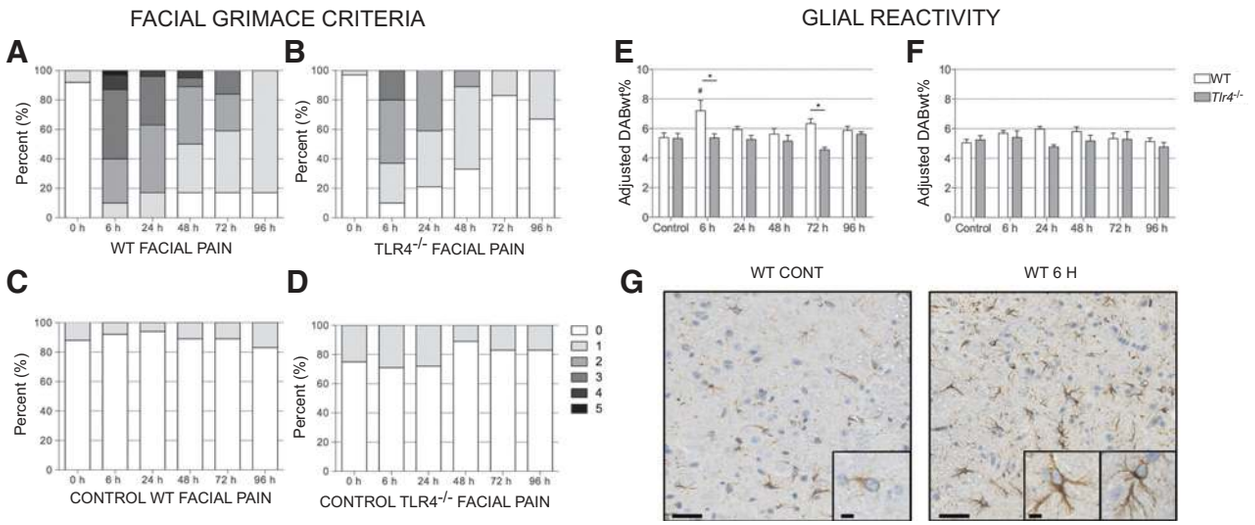

Figure 5.

Facial grimace criteria (A–D), GFAP staining (marker of astrocytic reactivity; E, G), and Iba-1 staining (marker of microglial reactivity; F) following irinotecan treatment. Facial grimace scores were assessed four times daily using the facial grimace criteria. Most significant facial pain was seen at 6 hours following treatment with irinotecan (A and B). Tlr4$^{-/-}$ mice had lower facial pain scores at all time points (***, $P < 0.0001$, 6–72 hours; *, $P = 0.0072$, 96 hours). GFAP and Iba-1 immunostaining was assessed in the dorsal column of the lumbar spinal cord. Increased astrocytic activation (GFAP) was seen in treated WT mice at 6 hours compared with controls (E; #, $P = 0.0041$). This was not evident in BALB/c-Tlr4$^{-/-billy}$ mice ($P > 0.05$). Irinotecan-treated WT mice showed increased GFAP staining compared with BALB/c-Tlr4$^{-/-billy}$ mice at 6 hours (*, $P = 0.008$) and 72 hours (*, $P = 0.012$). No change was seen in microglial activity (Iba-1) across the full time course in both WT and Tlr4$^{-/-}$ mice (F; $P > 0.05$). Data, mean ± SEM. G, representative images of GFAP staining in vehicle control WT mice and 6 hours after irinotecan. Scale bars, 50 μm or 10 μm for representative images and subset panels, respectively. Original magnification, ×40. WT mice treated with irinotecan displayed morphologic changes in astrocyte phenotype (somatic hypertrophy, thickened, and ramified processes) indicative of an activated state.

activation, was seen at 6 hours in WT animals compared with controls (#, $P = 0.004$; Fig. 5B). GFAP staining was significantly greater in WT than in BALB/c-*Tlr4*$^{-/-billy}$ mice at 6 (*, $P = 0.008$) and 72 hours (*, $P = 0.01$). No change was seen in Iba-1 staining in any animals (Fig. 5C; $P > 0.05$). Representative images (Fig. 5D) support activation of astrocytes with obvious changes in phenotype 6 hours after irinotecan in WT mice.

Irinotecan increases blood–brain barrier permeability to albumin

Elevated albumin staining was seen in WT (#, $P = 0.0001$) and BALB/c-*Tlr4*$^{-/-billy}$ mice (^, $P = 0.03$) at 24 hours, and in WT mice at 48 and 72 hours (#, $P = 0.006$ and #, $P = 0.03$, respectively; Fig. 6A), although there was no difference between WT and BALB/c-*Tlr4*$^{-/-billy}$ mice ($P > 0.05$). Both parenchymal (Fig. 6C) and perivascular (Fig. 6D) albumin was evident in WT and BALB/c-*Tlr4*$^{-/-billy}$ mice treated with irinotecan, with minimal leakage in control animals (Fig. 6B).

Discussion

TLR4 has been hypothesized to play a key role in the development of both chemotherapy-induced gut toxicity and pain (9, 15). Results from the current study support this newly proposed hypothesis, highlighting significant improvements in symptomatic parameters of gut toxicity and histopathologic markers in BALB/c-*Tlr4*$^{-/-billy}$ mice treated with irinotecan. This study is also the first to show paralleled improvements in *in vivo* pain markers and central glial reactivity following irinotecan.

The gut microbiota is critical in regulating the severity of gut toxicity, with increased levels of LPS-producing, gram-negative bacteria correlating with diarrhea severity (5, 29). Comparable levels of major phylogenies (fermicutes and bacteroidetes) were seen in WT and BALB/c-*Tlr4*$^{-/-billy}$ mice at baseline. However, small variations were seen in two relatively low-abundance microbes. These differences seen in the composition of the gut microbiome in WT and BALB/c-*Tlr4*$^{-/-billy}$ mice are not surprising given the wealth of emerging evidence indicating that both genetic and environment factors, such as breeding rooms// facilities, weigh significantly on the composition of the gut microbiome (30).

At baseline, TLR4 knockout mice exhibited higher levels of the TM7 bacterial phyla. Little is known about this bacterial phylogeny; however, it has been suggested to contribute to inflammatory pathologies within the gastrointestinal tract (31). More importantly, BALB/c-*Tlr4*$^{-/-billy}$ mice had elevated levels of β-glucuronidase-producing proteobacteria, likely increasing the rate of SN-38 reactivation, and thus worsened gut toxicity. Despite this predisposition, BALB/c-*Tlr4*$^{-/-billy}$ mice showed improvements in both the duration and severity of symptoms compared with WT mice. This finding complements recent research showing that germ-free mice experienced less severe irinotecan-induced gut toxicity compared with conventional mice (32). Most importantly, the germ-free mice also had higher levels of unbound SN-38 and higher β-glucuronidases activity. Comparatively, depletion of the gut microbiome with oral antibiotics has been shown to be effective in reducing irinotecan-induced diarrhea (33). It is now essential to determine if these improvements are the results of reduced microbial metabolism and SN-38 reactivation, or the result of reduced TLR4-mediated signaling. Determination of which factor contributes more significantly to clinical outcomes would therefore better direct therapeutic research efforts.

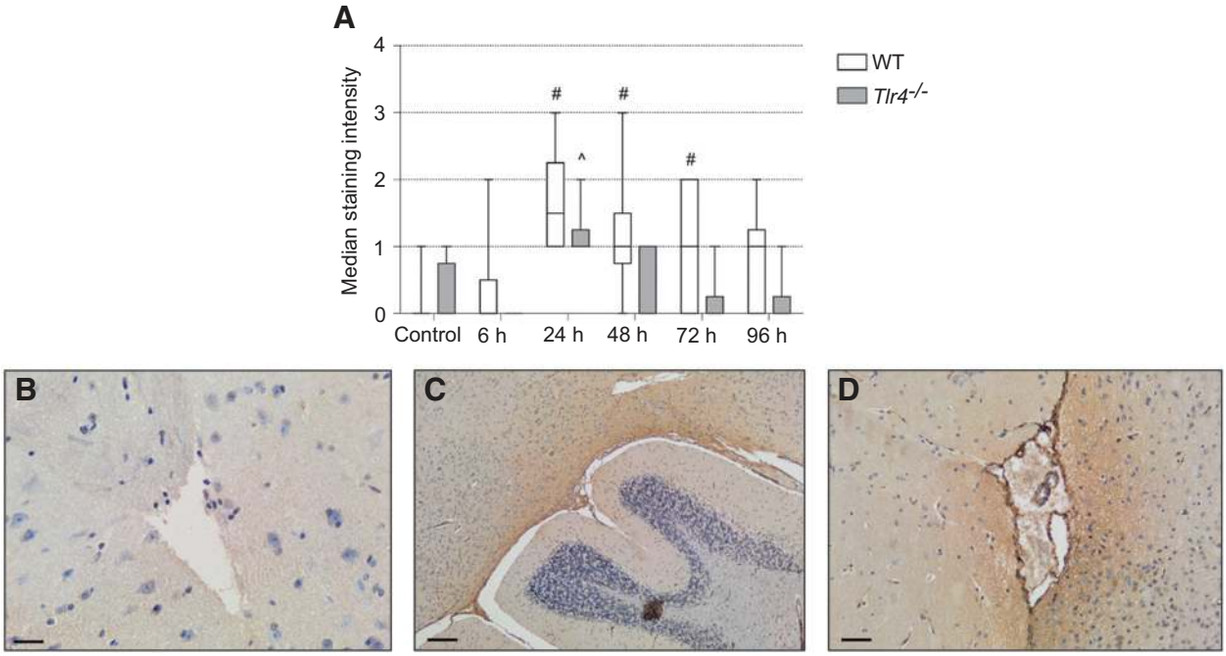

Figure 6.
Irinotecan causes blood–brain barrier dysfunction. Staining was analyzed using a semiquantitative 0–3 grading system and represented as interquartile range ± mix/max. A Kruskal–Wallis with *post hoc* testing was performed to identify statistical significance in nonparametric data. Scale bars, 20, 100, and 50 μm for B, C, and D, respectively. Original magnification, ×40. Albumin staining, indicative of increased blood–brain barrier transit, was elevated compared to untreated controls at 24 hours (#, $P < 0.0001$), 48 hours (#, $P = 0.0063$), and 72 hours (#, $P = 0.0325$) in WT mice; this was only seen at 24 hours (^, $P = 0.0325$) in BALB/c-*Tlr4*$^{-/-billy}$ mice. No differences were seen between WT and BALB/c-*Tlr4*$^{-/-billy}$ mice ($P > 0.05$). Qualitative assessment showed that albumin leakage was not limited to a particular brain region, but affected the vasculature globally with both parenchymal (C) and perivascular (D) albumin staining noted. Minimal leakage was observed in control animals (B).

Extensive literature exists showing the protective effect of TLR4 deletion in an inflammatory setting; however, this appears to be limited to only acute insults, with TLR4 deficiency exacerbating chronic inflammatory diseases (34). For example, significant improvements in acute inflammation have been shown in the absence of TLR4 and MyD88, a downstream signaling molecule of TLR, following acute infection with *Citrobacter rodentium* (34). Similar results have also been demonstrated in methotrexate-induced gut toxicity, with MD-2 (TLR4 accessory protein) deletion improving clinical and histologic parameters of toxicity (35). Importantly, this study showed that TLR4 and TLR2 appear to have opposing roles, with both genetic deletion and pharmacologic inhibition of TLR2 worsening methotrexate-induced damage (35). It appears that TLR2 has paradoxical roles in chemotherapy-induced gut toxicity, with improvements seen in *Tlr2*$^{-/-}$ mice treated with irinotecan. This study also showed that *Myd88*$^{-/-}$ mice were also protected from developing severe irinotecan-induced gut toxicity, reiterating the importance of TLR4-dependent signaling (35). Despite support for TLR4 deletion providing protection against chemotherapy-induced gut toxicity, this does not appear to be the case for acute and chronic colitis, with *Tlr4*$^{-/-}$ mice more susceptible to ulceration and bleeding (34). Although the unique mechanisms to each effect are not understood, these data do imply ambivalent roles for TLR4 in different inflammatory-based pathologies in the gastrointestinal tract.

It is well established that irinotecan-induced gut toxicity occurs through apoptosis of crypt epithelial cells through the gastrointestinal tract and consequently apoptosis is an established marker of toxicity severity (26). Our results showed significantly decreased levels of apoptosis in the jejunum and ileum of irinotecan-treated BALB/c-*Tlr4*$^{-/-billy}$ mice. This finding supports recent research suggesting that TLR4 signaling contributes to intestinal stem cell apoptosis through endoplasmic reticular stress-related mechanisms (36). We also saw that levels of proliferation inversely parallel these changes in cellular dynamics. This is of great clinical significance as apoptosis is one of the initial steps in the cascade of biologic events that results in the development of gut toxicity. If TLR4 deletion is able to profoundly impact such an early mediator of toxicity, it provides an excellent opportunity to intervene prior to architectural tissue damage, inflammation, and bacterial translocation.

In this study, increased FITC-dextran and endotoxin permeability were seen in irinotecan-treated WT mice, indicative of altered intestinal barrier function. Importantly, *Tlr4*$^{-/-}$ maintained intestinal barrier function with no significant changes in FITC-dextran permeability and decreased LPS translocation. Surprisingly, BALB/c-*Tlr4*$^{-/-billy}$ mice only showed mild improvements in serum endotoxin compared with WT mice and this did not appear to reflect the differences in intestinal damage. The failure to show differences at most time points in this study could be explained by evidence suggesting that TLR4 on hepatocytes is required for complete endotoxin clearance (37).

Reducing bacterial translocation has profound implications for systemic inflammatory responses and the exacerbation of direct mucosal cytotoxicity. Highlighting this pathobiologic mechanism, BALB/c-*Tlr4*$^{-/-billy}$ mice displayed less severe intestinal inflammation than WT mice. The most significant difference was seen for IL6, in which BALB/c-*Tlr4*$^{-/-billy}$ mice showed no increase

after treatment, supporting the idea that TLR4-dependent NFκB activation is required for the release of IL6 from macrophages (38). Stunted IL6 production has also been seen in MyD88-deficient mice (39) and *Tlr4*$^{-/-}$ macrophages (40).

The current study also identified, for the first time, disruption of the blood–brain barrier in animals treated with irinotecan. Blood–brain barrier disruption has been hypothesized to contribute to the development of "chemobrain" and cognitive impairment seen following chemotherapy, allowing cytotoxic agents direct access to the CNS (41). It has also been suggested that uncontrolled blood–brain barrier transit may potentiate the ability of peripheral inflammation to influence central pain signaling. It is becoming increasingly recognized that TLR4, expressed on centrally located glia, is able to recognize and respond to peripherally derived LPS and inflammatory mediators (9). We have shown translocation of LPS to systemic circulation following chemotherapy treatment, reflecting the swing toward a gram-negative, pathogenic gut microbiome profile following chemotherapy. Despite this, we saw no association with serum LPS, glial activation, and pain. Instead, astrocytic activation appeared to occur bimodally, with increases in GFAP staining seen at 6 and 72 hours. This suggests that cellular events associated with apoptosis (which peaks at 6 hours) or inflammation may be more important in TLR4-mediated glial activation. This concept is particularly compelling when looking at recent research by Ji and colleagues (2013) who reported significant astrocytic hypertrophy and activation in the dorsal horn of vincristine-treated rats with mechanical allodynia (42). Treatment with pentoxifylline, an anti-inflammatory agent, attenuated astrocytic reactivity and mechanical allodynia. Astrocytic reactivity has also been identified in the lumbar spinal cord of rats receiving oxaliplatin treatment, providing evidence linking peripheral inflammation and central gliosis. It is now critical to determine if the irinotecan-induced gut toxicity and pain are independent, yet simultaneously occurring events that are both governed by TLR4, or if there is a true directional mechanism linking one to the other.

Data from the current study have clearly highlighted the involvement of TLR4 in the development of irinotecan-induced gut toxicity and pain and provide a unique opportunity to simultaneously treat irinotecan-induced toxicities. In all cases of TLR4-targeted therapeutic options, the effect on both the efficacy of the anticancer therapy and overall tumor kinetics is paramount. This is particularly the case when targeting TLR4, as recent evidence now suggests that it may play critical roles in tumor growth. For example, Apetoh and colleagues (2007) showed that TLR4-deficient animals had increased tumor growth under normal conditions and in response to doxorubicin (43). TLR4 inhibition has also been implicated in tumor regression, with several studies now showing that numerous cancer cell lines [e.g., SW260 (colon), CRC-526 (breast), PC3 (prostate)] overexpress TLR4 and that LPS stimulates their growth (44–46). In addition, although not assessed in the current study, future work will need to clarify the role of TLR4 in normal gastrointestinal motility patterns given recent research implicating TLR4 in altered motility patterns following opioid treatment (47, 48).

Conclusions

Given the ubiquitous involvement of the innate immune system, particularly TLR4, in gut homeostasis and central pain signaling, it presents as a potentially overlooked candidate in the treatment of chemotherapy-induced gut toxicity and pain. Our research has demonstrated that TLR4 is pivotal in the development of both toxicities. This research not only improves our understanding of the underlying mechanisms involved, but also reveals a promising opportunity to intervene in the complex pathophysiology of these dose-limiting side effects of chemotherapy. Research efforts must now be targeted at tailoring methods of inhibiting TLR4, keeping in mind the potential effects on tumor burden and gastrointestinal function.

Disclosure of Potential Conflicts of Interest

R.J. Gibson reports receiving a commercial research grant from and is a consultant/advisory board member for Onyx Pharmaceuticals. No potential conflicts of interest were disclosed by the other authors.

Authors' Contributions

Conception and design: H.R. Wardill, R.J Gibson, J.K. Coller, M.R. Hutchinson, J.M. Bowen

Development of methodology: H.R. Wardill, M.R. Hutchinson, J.M. Bowen

Acquisition of data (provided animals, acquired and managed patients, provided facilities, etc.): H.R. Wardill, Y.Z.A. Van Sebille, K.R. Secombe, I.A. White, V. Staikopoulos, J.M. Bowen

Analysis and interpretation of data (e.g., statistical analysis, biostatistics, computational analysis): H.R. Wardill, R.J Gibson, K.R. Secombe, J.K. Coller, M.R. Hutchinson

Writing, review, and/or revision of the manuscript: H.R. Wardill, R.J Gibson, Y.Z.A. Van Sebille, J.K. Coller, J. Manavis, M.R. Hutchinson, V. Staikopoulos, R.M. Logan, J.M. Bowen

Administrative, technical, or material support (i.e., reporting or organizing data, constructing databases): K.R. Secombe, J. Manavis, M.R. Hutchinson

Study supervision: R.J Gibson, R.M. Logan, J.M. Bowen

Acknowledgments

The authors thank Mr. Anthony Wignall for his help in conducting the animal study, as well as Professor Paul Foster from the University of Newcastle for supplying the TLR4 null mice.

Grant Support

H.R. Wardill was supported by Florey Medical Research Foundation Doctor Chun Chung Wong and Madam So Sau Lam Memorial Postgraduate Cancer Research Top Up Scholarship 2015. H.R. Wardill and Y.Z.A Van Sebille were supported by Australian Postgraduate Award. R.J. Gibson, J.K Coller, and J.M Bowen were supported by Ray and Shirl Norman Cancer Research Trust Project Grant. M.R. Hutchinson received Australian Research Council Research Fellowship (DP110100297).

The costs of publication of this article were defrayed in part by the payment of page charges. This article must therefore be hereby marked *advertisement* in accordance with 18 U.S.C. Section 1734 solely to indicate this fact.

Received December 23, 2015; revised February 29, 2016; accepted March 17, 2016; published OnlineFirst March 29, 2016.

References

1. Lalla RV, Bowen J, Barasch A, Elting L, Epstein J, Keefe DM, et al. MASCC/ISOO clinical practice guidelines for the management of mucositis secondary to cancer therapy. Cancer 2014;120:1453–61.
2. Carlotto A, Hogsett VL, Maiorini EM, Razulis JG, Sonis ST. The economic burden of toxicities associated with cancer treatment: review of the literature and analysis of nausea and vomiting, diarrhoea, oral mucositis and fatigue. PharmacoEconomics 2013;31:753–66.
3. Sonis ST. The pathobiology of mucositis. Nat Rev Cancer 2004;4:277–84.
4. Chabot GG. Clinical pharmacokinetics of irinotecan. Clin Pharmacokinet 1997;33:245–59.

5. Stringer AM, Gibson RJ, Logan RM, Bowen JM, Yeoh AS, Keefe DM. Faecal microflora and beta-glucuronidase expression are altered in an irinotecan-induced diarrhea model in rats. Cancer Biol Ther 2008; 7:1919–25.
6. Stringer AM, Gibson RJ, Bowen JM, Logan RM, Ashton K, Yeoh AS, et al. Irinotecan-induced mucositis manifesting as diarrhoea corresponds with an amended intestinal flora and mucin profile. Int J Exp Pathol 2009; 90:489–99.
7. Stringer AM, Gibson RJ, Logan RM, Bowen JM, Yeoh AS, Hamilton J, et al. Gastrointestinal microflora and mucins may play a critical role in the development of 5-Fluorouracil-induced gastrointestinal mucositis. Exp Biol Med 2009;234:430–41.
8. Wardill HR, Gibson RJ, Logan RM, Bowen JM. TLR4/PKC-mediated tight junction modulation: a clinical marker of chemotherapy-induced gut toxicity? Int J Cancer 2014;135:2483–92.
9. Wardill HR, Van Sebille YZ, Mander KA, Gibson RJ, Logan RM, Bowen JM, et al. Toll-like receptor 4 signaling: a common biological mechanism of regimen-related toxicities: an emerging hypothesis for neuropathy and gastrointestinal toxicity. Cancer Treat Rev 2015;41:122–8.
10. Al-Dasooqi N, Sonis ST, Bowen JM, Bateman E, Blijlevens N, Gibson RJ, et al. Emerging evidence on the pathobiology of mucositis. Support Care Cancer 2013;21:2075–83.
11. Fukata M, Michelsen KS, Eri R, Thomas LS, Hu B, Lukasek K, et al. Toll-like receptor-4 is required for intestinal response to epithelial injury and limiting bacterial translocation in a murine model of acute colitis. Am J Physiol Gastrointest Liver Physiol 2005;288:G1055–65.
12. De Nardo D. Toll-like receptors: activation, signalling and transcriptional modulation. Cytokine 2015;74:181–9.
13. Jacobsen JH, Watkins LR, Hutchinson MR. Discovery of a novel site of opioid action at the innate immune pattern-recognition receptor TLR4 and its role in addiction. Int Rev Neurobiol 2014;118:129–63.
14. Bowen JM, Coller J, Hutchinson M, Gibson RJ. Expression of TLRs in the rat intestine following chemotherapy for cancer. Brain Behaviour Immunity 2012;26:S27–S.
15. Gibson RJ, Coller JK, Wardill HR, Hutchinson M, Smid SD, Bowen JM. Chemotherapy-induced gut toxicity and pain: involvement of TLRs. Support Care Cancer 2016;24:2251–8.
16. Aprile G, Ramoni M, Keefe D, Sonis S. Application of distance matrices to define associations between acute toxicities in colorectal cancer patients receiving chemotherapy. Cancer 2008;112:284–92.
17. Phipps S, Lam CE, Kaiko GE, Foo SY, Collison A, Mattes J, et al. Toll/IL-1 signaling is critical for house dust mite-specific helper T cell type 2 and type 17 [corrected] responses. Am J Respir Crit Care Med 2009;179:883–93.
18. Gibson RJ, Bowen JM, Alvarez E, Finnie J, Keefe DM. Establishment of a single-dose irinotecan model of gastrointestinal mucositis. Chemotherapy 2007;53:360–9.
19. Sotocinal SG, Sorge RE, Zaloum A, Tuttle AH, Martin LJ, Wieskopf JS, et al. The Rat Grimace Scale: a partially automated method for quantifying pain in the laboratory rat via facial expressions. Mol Pain 2011;7:55.
20. Mathijssen RH, van Alphen RJ, Verweij J, Loos WJ, Nooter K, Stoter G, et al. Clinical pharmacokinetics and metabolism of irinotecan (CPT-11). Clin Cancer Res 2001;7:2182–94.
21. Zhang J, Kobert K, Flouri T, Stamatakis A. PEAR: a fast and accurate Illumina Paired-End reAd mergeR. Bioinformatics 2014;30:614–20.
22. Caporaso JG, Kuczynski J, Stombaugh J, Bittinger K, Bushman FD, Costello EK, et al. QIIME allows analysis of high-throughput community sequencing data. Nat Methods 2010;7:335–6.
23. Edgar RC. Search and clustering orders of magnitude faster than BLAST. Bioinformatics 2010;26:2460–1.
24. Edgar RC, Haas BJ, Clemente JC, Quince C, Knight R. UCHIME improves sensitivity and speed of chimera detection. Bioinformatics 2011;27: 2194–200.
25. Howarth GS, Francis GL, Cool JC, Xu X, Byard RW, Read LC. Milk growth factors enriched from cheese whey ameliorate intestinal damage by methotrexate when administered orally to rats. J Nutr 1996;126:2519–30.
26. Keefe DM, Brealey J, Goland GJ, Cummins AG. Chemotherapy for cancer causes apoptosis that precedes hypoplasia in crypts of the small intestine in humans. Gut 2000;47:632–7.
27. Helps SC, Thornton E, Kleinig TJ, Manavis J, Vink R. Automatic nonsubjective estimation of antigen content visualized by immunohistochemistry using color deconvolution. Appl Immunohistochem Mol Morphol 2012; 20:82–90.
28. Bland M. The analysis of cross-tabulation. An introduction to medical statistics . 3rd ed. New York: Oxford University Press; 2005.
29. Stringer AM, Al-Dasooqi N, Bowen JM, Tan TH, Radzuan M, Logan RM, et al. Biomarkers of chemotherapy-induced diarrhoea: a clinical study of intestinal microbiome alterations, inflammation and circulating matrix metalloproteinases. Support Care Cancer 2013;21:1843–52.
30. Hufeldt MR, Nielsen DS, Vogensen FK, Midtvedt T, Hansen AK. Variation in the gut microbiota of laboratory mice is related to both genetic and environmental factors. Comp Med 2010;60:336–47.
31. Kuehbacher T, Rehman A, Lepage P, Hellmig S, Folsch UR, Schreiber S, et al. Intestinal TM7 bacterial phylogenies in active inflammatory bowel disease. J Med Microbiol 2008;57:1569–76.
32. Pedroso SH, Vieira AT, Bastos RW, Oliveira JS, Cartelle CT, Arantes RE, et al. Evaluation of mucositis induced by irinotecan after microbial colonization in germ-free mice. Microbiology 2015;161:1950–60.
33. Kurita A, Kado S, Matsumoto T, Asakawa N, Kaneda N, Kato I, et al. Streptomycin alleviates irinotecan-induced delayed-onset diarrhea in rats by a mechanism other than inhibition of beta-glucuronidase activity in intestinal lumen. Cancer Chemother Pharmacol 2011;67:201–13.
34. Gibson DL, Ma C, Bergstrom KS, Huang JT, Man C, Vallance BA. MyD88 signalling plays a critical role in host defence by controlling pathogen burden and promoting epithelial cell homeostasis during Citrobacter rodentium-induced colitis. Cell Microbiol 2008;10:618–31.
35. Frank M, Hennenberg EM, Eyking A, Runzi M, Gerken G, Scott P, et al. TLR signaling modulates side effects of anticancer therapy in the small intestine. J Immunol 2015;194:1983–95.
36. Afrazi A, Branca MF, Sodhi CP, Good M, Yamaguchi Y, Egan CE, et al. Toll-like receptor 4-mediated endoplasmic reticulum stress in intestinal crypts induces necrotizing enterocolitis. J Biol Chem 2014;289:9584–99.
37. Deng M, Scott MJ, Loughran P, Gibson G, Sodhi C, Watkins S, et al. Lipopolysaccharide clearance, bacterial clearance, and systemic inflammatory responses are regulated by cell type-specific functions of TLR4 during sepsis. J Immunol 2013;190:5152–60.
38. Pathak SK, Basu S, Bhattacharyya A, Pathak S, Banerjee A, Basu J, et al. TLR4-dependent NF-kappaB activation and mitogen- and stress-activated protein kinase 1-triggered phosphorylation events are central to Helicobacter pylori peptidyl prolyl cis-, trans-isomerase (HP0175)-mediated induction of IL-6 release from macrophages. J Immunol 2006;177:7950–8.
39. Hayashi F, Smith KD, Ozinsky A, Hawn TR, Yi EC, Goodlett DR, et al. The innate immune response to bacterial flagellin is mediated by Toll-like receptor 5. Nature 2001;410:1099–103.
40. Shoenfelt J, Mitkus RJ, Zeisler R, Spatz RO, Powell J, Fenton MJ, et al. Involvement of TLR2 and TLR4 in inflammatory immune responses induced by fine and coarse ambient air particulate matter. J Leukoc Biol 2009;86:303–12.
41. Holmes D. Trying to unravel the mysteries of chemobrain. Lancet Neurol 2013;12:533–4.
42. Ji XT, Qian NS, Zhang T, Li JM, Li XK, Wang P, et al. Spinal astrocytic activation contributes to mechanical allodynia in a rat chemotherapy-induced neuropathic pain model. PLoS One 2013;8:e60733.
43. Apetoh L, Ghiringhelli F, Tesniere A, Obeid M, Ortiz C, Criollo A, et al. Toll-like receptor 4-dependent contribution of the immune system to anticancer chemotherapy and radiotherapy. Nat Med 2007;13:1050–9.
44. Huang HY, Zhang ZJ, Cao CB, Wang N, Liu FF, Peng JQ, et al. The TLR4/NF-kappaB signaling pathway mediates the growth of colon cancer. Eur Rev Med Pharmacol Sci 2014;18:3834–43.
45. Yang H, Zhou H, Feng P, Zhou X, Wen H, Xie X, et al. Reduced expression of Toll-like receptor 4 inhibits human breast cancer cells proliferation and inflammatory cytokines secretion. J Exp Clin Cancer Res 2010;29:92.
46. Jain S, Suklabaidya S, Das B, Raghav SK, Batra SK, Senapati S. TLR4 activation by lipopolysaccharide confers survival advantage to growth factor deprived prostate cancer cells. Prostate 2015;75:1020–33.
47. Farzi A, Halicka J, Mayerhofer R, Frohlich EE, Tatzl E, Holzer P. Toll-like receptor 4 contributes to the inhibitory effect of morphine on colonic motility in vitro and in vivo. Sci Rep 2015;5:9499.
48. Anitha M, Vijay-Kumar M, Sitaraman SV, Gewirtz AT, Srinivasan S. Gut microbial products regulate murine gastrointestinal motility via Toll-like receptor 4 signaling. Gastroenterology 2012;143:1006–16e4.